

Carbon-free sandwich compounds based on arsenic and antimony with icosahedral metal cores

Received: 26 September 2022

Accepted: 16 January 2023

Published online: 20 February 2023

 Check for updatesXu-Hui Yue^{1,6}, Wei-Xing Chen^{1,6}, Tao Yang², Alvaro Muñoz-Castro³, Gernot Frenking^{4,5} & Zhong-Ming Sun¹✉

Traditionally, a metallocene complex comprises a metal centre sandwiched between two aromatic organic ligands and such complexes have been extensively investigated. Carbon-free analogues of metallocene with homoleptic As₅ or Sb₅ ligands, however, have remained experimentally elusive, especially analogues of higher nuclearity. Here we report the synthesis and characterization of sandwich-type clusters [Pn@M₁₂Pn₁₀(Pn₅)₂]^{4-/5-} (Pn = As, Sb; M = Co, Fe), where the endohedral icosahedral cluster [Pn@M₁₂] can be regarded as a spherical-like three-dimensional coordination centre surrounded by a Pn₁₀ ring and two Pn₅ pentagonal caps. Quantum chemical calculations reveal that the [Pn@M₁₂] has orbitals that mimic 1S, 1P and 1D electronic shells, which can interact with the outer (Pn₅)₂ ring layer. These interactions occur because the frontier orbitals are dominated by the (n - 1)d block orbitals of the metal atoms. The π₁-As₅ orbitals interact with 1S and part of the 1P shell of the central core, while the π₂- and π₃-As₅ orbitals interact with the symmetry-allowed part of the 1P and 1D shells. The characteristics of this orbital interaction are analogous to those of mononuclear metallocenes.

Ferrocene (**I** in Fig. 1) and its derivatives, namely metallocenes, with sandwich-type structures comprising a mononuclear metal centre between two organic conjugated ligands, have been intensively investigated¹⁻⁴. Metallocenes have been widely used in the fields of catalysis, medicine, batteries and other materials science applications⁵⁻⁹. Subsequently, studies have extended the range of sandwich complexes to species with carbon-free inorganic ligands. The replacement of CH fragments in cyclopentadiene by isoelectronic phosphorus or arsenic atoms leads to heterocyclopentadienyl [(RC)_nP_{5-n}]⁻ ligands (n = 0-4), which have markedly different chemical properties compared to their all-carbon analogues and can be used to construct a series of heteroferrocenes¹⁰⁻¹⁷. These kinds of complexes could serve as efficient

starting materials for the syntheses of diverse organometallic compounds and show activity in catalysis¹⁸.

Although mixed-sandwich complexes have long been isolated, attempts to synthesize a carbon-free all-phosphorus metallocene failed until [Ti(η⁵-P₅)₂]²⁻ (**II** in Fig. 1), which has enhanced π-acceptor properties compared with all-carbon analogues¹⁹. Very recently, the all-phosphorus sandwich complex [Fe(η⁴-P₄)₂]²⁻ has been proved to be the closest ferrocene analogue so far to the decaphosphoferrocene²⁰. In contrast, in the case of the heavier analogues of group 15, arsenic and antimony, the difficulties are more pronounced, and thus only a few pentaarsaferrocene derivatives [(η⁵-As₅)Fe(η⁵-C₅Me₄R)] (R = Me, Et) (**III** in Fig. 1) with one η⁵-bonded *cyclo*-As₅⁻ ligand²¹ and

¹State Key Laboratory of Elemento-organic Chemistry, Tianjin Key Lab of Rare Earth Materials and Applications, School of Material Science and Engineering, Nankai University, Tianjin, China. ²MOE Key Laboratory for Non-equilibrium Synthesis and Modulation of Condensed Matter, School of Physics, Xi'an Jiaotong University, Xi'an, China. ³Facultad de Ingeniería, Arquitectura y Diseño, Universidad San Sebastián, Santiago, Chile. ⁴Donostia International Physics Center (DIPC), Donostia, Spain. ⁵Fachbereich Chemie, Philipps-Universität Marburg, Marburg, Germany. ⁶These authors contributed equally: Xu-Hui Yue, Wei-Xing Chen. ✉e-mail: sunlab@nankai.edu.cn

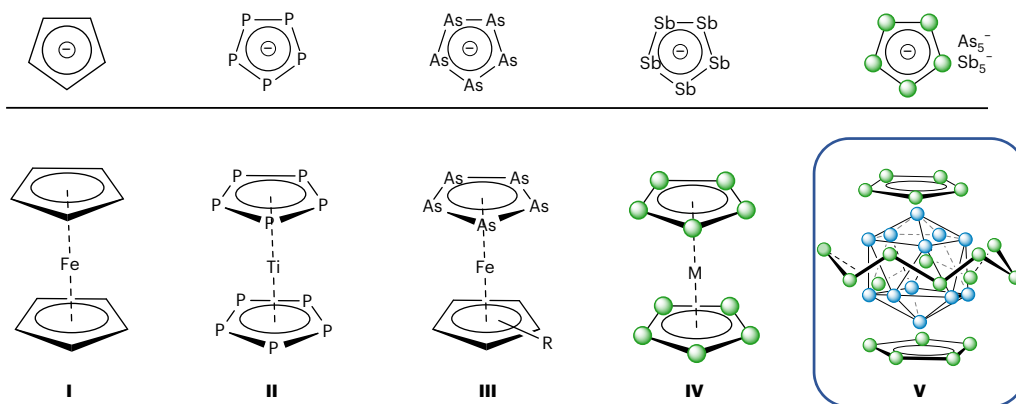


Fig. 1 | Selected examples of known and predicted sandwich complexes with cyclopentadienyl or cyclo- P_5 , cyclo- As_5 and cyclo- Sb_5 ligands. **I**, $Fe(\eta^5-C_5H_5)_2$ (ref. 1); **II**, $[Ti(\eta^5-P_5)_2]^{2-}$ (ref. 19); **III**, Cp^RFeAs_5 ($Cp^R = C_5Me_5, C_5Me_4Et$) (refs. 22,23);

IV, theoretically predicted sandwich structures $[M(Pn_5)_2]^{q-}$ ($Pn = As, Sb; M = Ti, q = 2; M = Fe, q = 0$)^{24,25}; **V**, $[Pn@M_{12}Pn_{10}(Pn_5)_2]^{q-}$ ($Pn = As, M = Co, q = 4, 5; Pn = Sb, M = Fe, q = 5$).

organometallic compounds containing cyclo- As_5^- and cyclo- Sb_5^- rings are known^{22,23}.

Theoretical calculations confirm that homoleptic sandwich-like complexes $[Ti(Pn_5)_2]^{2-}$ and $Fe(Pn_5)_2$ ($Pn = As, Sb$) (**IV** in Fig. 1) are likely to be isolable, which has further stimulated the search for a sandwich complex with two cyclo- Pn_5^- ligands^{24,25}. The calculations show that heavier analogues of group 15 have lower dissociation energy, which means that the destabilizing factor will increase, posing a challenge to experimental isolation. This is the primary reason why these cyclo- As_5^- or cyclo- Sb_5^- flanked compounds via η^5 -ligated coordination mode have so far remained elusive.

The discovery of polymetallic interlayered complexes has expanded the new category of sandwich complexes²⁶. Further studies have found that small carbon ligands are not enough to cover the coordination space of the metal centre when the two-dimensional interlayer evolves into a three-dimensional (3D) metal cluster²⁷. However, larger-sized inorganic ligands composed of heavy elements are promising for solving the challenge of matching large-sized cores with the π orbitals of the cyclo-ligands^{28–30}. Here we report a series of sandwich-type complexes $[As@Co_{12}As_{10}(As_5)_2]^{4-/5-}$ and $[Sb@Fe_{12}Sb_{10}(Sb_5)_2]^{5-}$ (**V** in Fig. 1) by a Zintl ion synthesis strategy, in which an icosahedral cluster core $[Pn@M_{12}]$ ($Pn = As, Sb; M = Co, Fe$) serves as structural support displaying a discrete electronic shell structure involved in the stabilization of the outer structural layer, mimicking isolated transition metals. Interestingly, the cluster exhibits a different geometry compared with the known ‘onion-type’ or ‘matryoshka-type’ clusters $[E@M_{12}@E_{20}]^{n-}$ ($E = As/Sb/Sn, M = Ni/Pd/Cu, n = 3/4/12$) with similar $[E@M_{12}]$ cores^{31–34}. The outer layer of the former depicts a Pn_{10} ring in the equatorial plane, which is sandwiched between two inorganic aromatic cyclo- Pn_5^- ligands, while those of the latter can be described as undivided E_{20} shells. This series of complexes represent carbon-free sandwich complexes with 3D metal cores, extending the scope of the concept of mononuclear sandwich complexes to cluster-coordination-centred sandwich complexes.

Results and discussion

Synthesis of compounds **1**–**3**'

The compounds $\{[K(18\text{-crown-6})](en)_2[As@Co_{12}As_{10}(As_5)_2]\}$ (**1**) and $\{K_2[K(18\text{-crown-6})](en)_2\}[K(18\text{-crown-6})_2[As@Co_{12}As_{10}(As_5)_2]]\}$ (**2**) were obtained by reacting K_5As_4 with $Co(PPh_3)_2Cp$ in ethylenediamine (*en*) at 75 °C in the presence of 18-crown-6 (Supplementary Fig. 1). The compounds were isolated as black plate-like crystals and black block crystals with yields of 14% and 12%, respectively. Variation of molar ratio affords two compounds, $[As@Co_{12}As_{10}(As_5)_2]^{4-}$ (**1**) and $[As@Co_{12}As_{10}(As_5)_2]^{5-}$ (**2**), which carry negative charges of 4– and

5–, respectively. Correspondingly, under similar reaction conditions, the Fe/Sb binary sandwich-type $[Sb@Fe_{12}Sb_{10}(Sb_5)_2]^{5-}$ (**3a**) along with ‘onion-type’ $[Sb@Fe_{12}@Sb_{20}]^{5-}$ (**3b**) anions co-crystallized in the salt of $[K_3(18\text{-crown-6})_3(en)_2][K(18\text{-crown-6})(en)]_2$ **3a**_{0.745}**3b**_{0.255} (**3'**) (Supplementary Figs. 7–9). This compound was successfully isolated on reaction of K_5Sb_4 and 1,1'-bis(diphenylphosphino)ferrocene (DPPF), resulting in black block crystals with approximately 15% yield. In addition, when ferrocene instead of DPPF was used as starting reagent, no crystals of **3'** are isolated under the same conditions.

Characterization

Single-crystal X-ray diffraction reveals that all anionic clusters crystallize in the triclinic space group $P\bar{1}$ (see Supplementary Tables 1–4 for detailed crystallographic data and bond parameters). It is worth noting that the above isolated species **1–3a** are isostructural; clusters **1** and **2** have minor differences in bond lengths (Supplementary Tables 2 and 3), and thus the following discussion will mainly focus on cluster **2**. Cluster anion **3a** together with **1** and **2** can be interpreted overall as sandwich complexes with D_{5d} symmetry, where the endohedral icosahedron $[Pn@M_{12}]$ ($Pn = As, Sb; M = Co, Fe$) serves as a cluster-based coordination centre, located between two staggered cyclo- Pn_5 ligands, which is further surrounded by an equatorial puckered Pn_{10} ring (Fig. 2a–c). In the case of **3b**, this core–shell geometry is isostructural with the known ‘onion-type’ or ‘matryoshka-type’ clusters of formula $[E@M_{12}@E_{20}]^{n-}$ ($E = As, Sb, Sn; M = Ni, Pd, Cu; n = 3, 4, 12$)^{31–34}. Neither endohedral Co_{12} nor Fe_{12} icosahedral structures appear to have been synthesized in the solid state, although it has been predicted theoretically that such clusters may be stable^{35,36}.

In the $[As@Co_{12}]$ and $[Sb@Fe_{12}]$ subunits, the Co–Co and Fe–Fe bond distances fall in narrow ranges of 2.627(2)–2.696(2) Å and 2.609(2)–2.638(2) Å, respectively, showing an almost ideal icosahedron with I_h symmetry (Fig. 2h). The average heights d (namely, the distances between the two capping atoms of the bicapped pentagon antiprism) of the icosahedra are almost identical ($d_{Co} = 5.059$ Å, $d_{Fe} = 4.984$ Å), indicating that the closo-polyhedra $[As@Co_{12}]$ and $[Sb@Fe_{12}]$ are similarly sized. In addition, the Co–As contacts between the central arsenic atom and the 12 cobalt atoms (2.4486(16)–2.5541(17) Å) are slightly longer than the remaining Co–As distances (2.356(2)–2.417(2) Å). In cluster **1–3a**, each of the apical M atoms of the icosahedral core is coordinated to the cyclo- Pn_5^- ligand via the η^5 -coordination mode, while the other M atoms coordinate only with the four surrounding Pn atoms. This is different from **3b** and the reported $[As@Ni_{12}@As_{20}]^{3-}$ (ref. 31) and $[Sb@Pd_{12}@Sb_{20}]^{n-}$ ($n = 3, 4$)^{32,33}, in which each of the M atoms is coordinated with the surrounding arsenic or antimony atoms via the η^2 -coordination mode. Each triangular face of the icosahedron

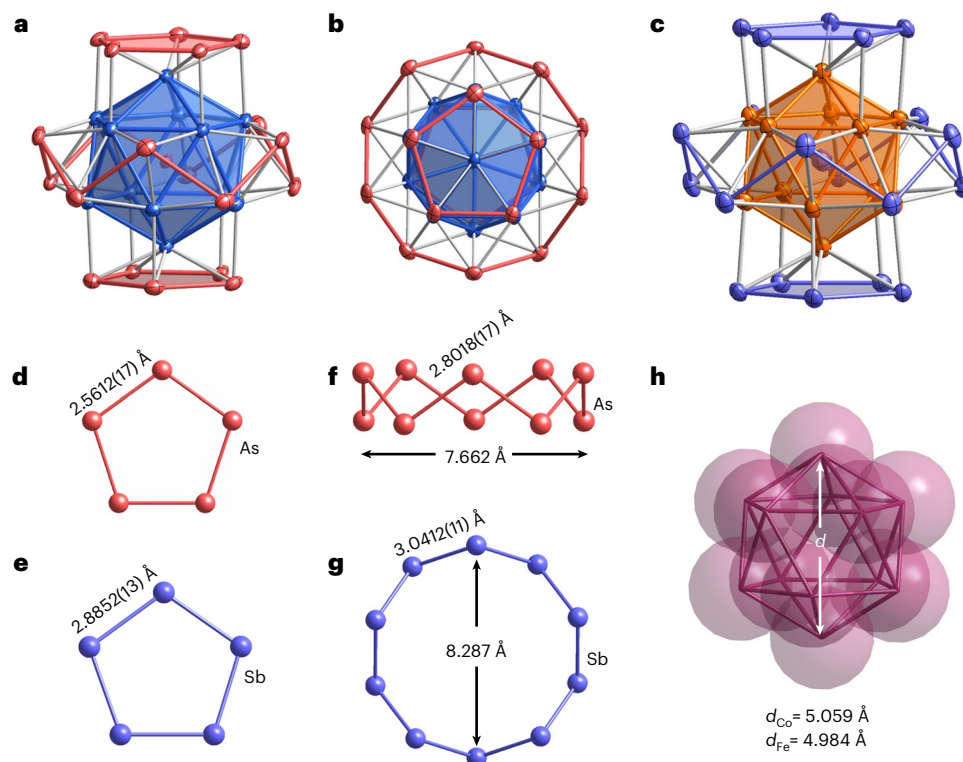


Fig. 2 | Molecular structures of the cluster anions $[\text{Pn}@M_{12}\text{Pn}_{10}(\text{Pn}_5)_2]^{5-}$ ($\text{Pn} = \text{As}, \text{Sb}; \text{M} = \text{Co}, \text{Fe}$) and their selected fragments. **a, b, Solid-state structures of anion **2**, $[\text{As}@M_{12}\text{As}_{10}(\text{As}_5)_2]^{5-}$, in two different orientations: side view (**a**) and top view (**b**). **c**, Solid-state structures of anion **3a**, $[\text{Sb}@M_{12}\text{Sb}_{10}(\text{Sb}_3)_2]^{3-}$, in side view. Displacement ellipsoids with 50% probability. **d–g**, The fragments of cyclo- Pn_5 (As_5 , **d**; Sb_5 , **e**) and puckered Pn_{10} ring**

(side view of As_{10} , **f**; top view of Sb_{10} , **g**) in cluster anions **2** and **3a**. The numbers displayed represent the corresponding selected bond lengths and dimensions (average values). **h**, Space-filling structure of the icosahedral M_{12} ($M = \text{Co}, \text{Fe}$) core; their dimensions d are given as average data. As, red; Sb, purple; Co, blue; and Fe, orange.

is capped by a Pn atom originating from the equatorial Pn_{10} ring. The average bond distance between the apical cobalt and five arsenic atoms of the cyclo- As_5^- is 2.381(2) Å, which is comparable to that between the waist cobalt atoms and the arsenic atoms in the equatorial As_{10} fragment (average, 2.358(2) Å). However, the distances of the waist cobalt atoms of the Co_{12} icosahedron to the arsenic atoms in the cyclo- As_5^- (average, 2.298(2) Å) are significantly shorter, indicating that there is a strong interaction between the Co_{12} core and the cyclo- As_5^- ligand in the vertical direction. From another perspective, each Pn atom in the Pn_5 rings is in a μ_2 -bridging mode to the M atoms in the M_{12} core, whereas that in the Pn_{10} ring is in a μ_3 -bridging mode. Although the rotation of the Pn_5 rings in **1–3a** gives rise to ‘onion-type’ $[\text{E}@M_{12}@E_{20}]^{n-}$ ($\text{E} = \text{Sb}, \text{M} = \text{Fe}$, **3b**; $\text{E} = \text{As}, \text{M} = \text{Ni}$; $\text{E} = \text{Sb}, \text{M} = \text{Pd}$)^{31–33}, the bonding conditions are different, and each of the E atoms in E_{20} coordinates with the M_{12} nucleus in the μ_3 -bridging mode. There is a significant change in the dimension of these isostructural sandwich compounds when the ligand is converted from arsenic to antimony. As shown in Fig. 2d–g, there are striking differences in the average Pn–Pn lengths of the cyclo- Pn_5^- ligands and the equatorial puckered Pn_{10} rings and in the size of the equatorial ring cavity. In the capping cyclo- As_5^- rings in **2**, the bond distances (2.5447(17)–2.5612(17) Å) fall within a narrow range (<0.02 Å) and are longer than those of $(\eta^5\text{-As}_5)\text{Fe}(\eta^5\text{-C}_5\text{Me}_4\text{Et})$ (2.316 Å)²¹. The uniform bond distances and bond angles (106.31(6)°–109.49(6)°) imply a delocalized aromatic property in the cyclo- As_5^- plane. The As–As bonds in the equatorial puckered As_{10} subunit (average, 2.8018(17) Å) are comparable to those in $[\text{As}@M_{12}@M_{20}]^{3-}$ (average, 2.752 Å)³¹ and much longer than that in the two cyclo- As_5^- ligands. Such bond elongation may be attributed to the high coordination number with the $[\text{E}@M_{12}]$ core. Moreover, compared to the As–As distances

in $[\text{As}@M_{12}@M_{20}]^{3-}$ (ref. 31) (average, 2.755 Å), the closest distance between the As_5 ring and equatorial As_{10} ring (average values of 3.490(16) Å for **1** and 3.474(19) Å for **2**) is much longer, indicating that As_{20} shells in ‘onion-type’ cluster are divided into As_5 and As_{10} fragments in anions **1** and **2** to form sandwich-type clusters.

Electrospray ionization mass spectrometry (ESI-MS) of an acetonitrile solution of the crystals of $\{[\text{K}(\text{18-crown-6})]_2(\text{en})\}_2[\text{As}@M_{12}\text{As}_{10}(\text{As}_5)_2]$ (**1'**) was performed in negative-ion mode. A series of ion peaks $[\text{Co}_{12}\text{As}_{21}]^-$, $[\text{KCo}_{12}\text{As}_{21}]^-$, $\{[\text{K}(\text{18-C-6})][\text{Co}_{12}\text{As}_{21}]^-\}$ and $\{[\text{K}(\text{18-C-6})]_2[\text{Co}_{12}\text{As}_{21}]\}^-$, containing the parent anion, were found, which indicates the high stability of the compound in gas-phase conditions. Additionally, ion peaks losing one or two arsenic atom(s) from the parent compound also appeared in the spectrum (Supplementary Fig. 10). The elemental composition of compounds **1'–3'** were confirmed by means of energy dispersive X-ray (EDX) analyses (Supplementary Figs. 16–18). Cluster **1** has 217 total electrons to form a paramagnetic complex, but all attempts to obtain the EPR signals failed. Theoretical calculations show that this phenomenon is attributable to cluster **1** favouring the high-spin $S = 7/2$ state rather than the $S = 1/2$ state for tetra anions (Supplementary Table 6), and this phenomenon has also been observed in the known anionic cluster³⁷.

Computational analysis

The structures of **1** and **2** show D_{5d} symmetry due to the spatial disposition of the external As_{20} layer as two As_5 rings and an equatorial As_{10} ring, retaining an almost perfect icosahedral $[\text{As}@M_{12}]$ core, as denoted by the continuous shape measures³⁸ with an r.m.s. deviation of 0.017 Å from a perfect icosahedron. The obtained sandwich-like D_{5d} symmetry in **1**, in its favoured 7/2 spin state is preferred over the

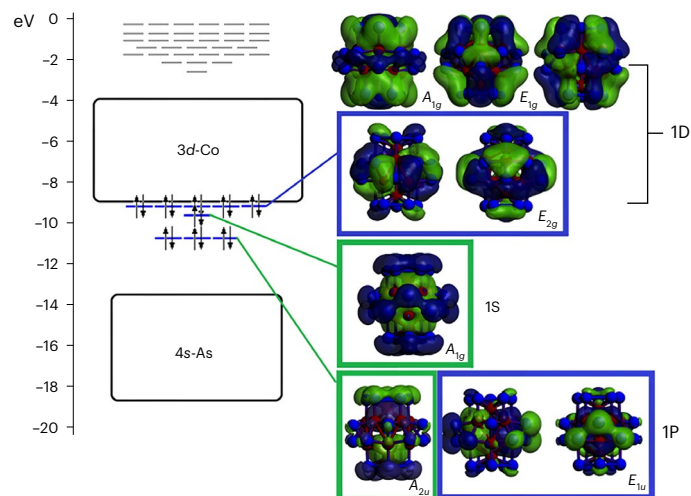


Fig. 3 | Selected orbitals revealing the bonding interaction in $[\text{As}@\text{Co}_{12}@\text{As}_{10}(\text{As}_5)_2]^{4+}$. Color code: Green boxes denote the 1S and 1P interaction with $\pi_1^- \text{As}_5$ and blue boxes denote the 1P and 1D interaction with π_2^- and $\pi_3^- \text{As}_5$ orbitals.

more spherical I_h symmetry by 31.8 kcal mol⁻¹ due to a more efficient bonding towards two As_5 units, in contrast to the matryoshka $[\text{As}@\text{Ni}_{12}@\text{As}_{20}]^{3-}$ (ref. ³¹) and $[\text{Sn}@\text{Cu}_{12}@\text{Sn}_{20}]^{12-}$ (ref. ³⁴) inter-metalloids. This situation suggests the plausible description of an all-inorganic analogue to metallocenes, involving an $[\text{As}@\text{Co}_{12}]$ central core acting as the coordination centre.

The sandwich-like arrangement of the outer $\text{As}_{10}(\text{As}_5)_2$ shell leads to an asymmetric charge distribution, according to the Hirshfeld charge analysis, with the equatorial As_{10} ring carrying $-1.31e$, and the $(\text{As}_5)_2$ fragments carrying an overall charge of $-0.72e$, denoting less electron-sharing towards the $[\text{As}@\text{Co}_{12}]$ ($-1.97e$) core. This situation is contrary to the hypothetical I_h -symmetry case where the outer layer As_{20} carries $-1.81e$, and the $[\text{As}@\text{Co}_{12}]$ core $-2.19e$. For $[\text{Sb}@\text{Fe}_{12}\text{Sb}_{10}(\text{Sb}_5)_2]^{5-}$, the I_h/D_{5d} difference is computed to be 24.3 kcal mol⁻¹, favouring the sandwich complex arrangement, with both species favouring a spin-state of 7/2, as denoted for D_{5d} species in Supplementary Table 6. This energy difference is lower than the calculated one for **1**, suggesting a more facilitated D_{5h}/I_h interconversion involving **3a** and **3b**. Similar to **1**, **3a** shows an equatorial Sb_{10} ring carrying more negative charge ($-1.49e$) than the overall charge from $(\text{Sb}_5)_2$ fragments ($-1.10e$), involving $-2.28e$ ascribed to the $[\text{Sb}@\text{Fe}_{12}]$ core, which varies between $-2.59e$ for the Sb_{20} outer layer and $-2.41e$ for the $[\text{Sb}@\text{Fe}_{12}]$ core in the more symmetric **3b** counterpart.

Taking cluster **1** as an example, the main bonding scheme towards the $6\pi\text{-As}_5^-$ rings is revealed via an orbital analysis showing that the main interaction is located in low-lying occupied orbitals where the π_1^- , π_2^- and $\pi_3^- \text{As}_5$ orbitals are collectively donating charge towards the 4s Co orbitals of the core, resulting in their stabilization—behaviour that can be ascribed to them being analogues of the 1S, 1P and 1D electronic shells (Fig. 3 and Supplementary Fig. 19)³⁹. The high-lying occupied orbitals are composed of the partially occupied 3d Co block orbitals, leading to the high-spin state. This situation is similar to the one described recently for carbonyl platinum clusters by Wei⁴⁰. The $\pi_1^- \text{As}_5$ orbitals interact with the 1S and part of the 1P shell ($1P_z$) from the central core, and the π_2^- and $\pi_3^- \text{As}_5$ orbitals interact with a part of 1P ($1P_x, 1P_y$) and 1D ($1D_{xz}, 1D_{yz}$), similar to a classical single-metal sandwich structure, and analogous to pentaarsaferrocene. Hence, $D_{5d}\text{-}[\text{As}@\text{Co}_{12}@\text{As}_{10}(\text{As}_5)_2]^{4+}$ appears to be the first cluster analogue to a sandwich complex based on a central icosahedral core as the coordination centre. Neighbour charge states, namely -3 and -5 , lead to favoured high-spin species ($S = 4/2$) by 64.2 and 15.7 kcal mol⁻¹, in comparison to the closed-shell state ($S = 0$).

For such species, the bonding towards both As_5 rings remains similar to the parent -4 charge state due to the fact that frontier orbitals are composed of 3d-block orbitals.

To compare the chemical bonding between the coordination centre and ligands in current sandwich complexes $[\text{Pn}@\text{M}_{12}\text{Pn}_{10}(\text{Pn}_5)_2]^{4-/5-}$ ($\text{Pn} = \text{As}, \text{Sb}; \text{M} = \text{Co}, \text{Fe}$) with classical mononuclear sandwiched ferrocene $\text{Fe}(\eta^5\text{-C}_5\text{H}_5)_2$ (**I**) and $[\text{Ti}(\eta^5\text{-P}_5)_2]^{2-}$ (**II**), an energy decomposition analysis (EDA) was performed. The cluster-based coordination centre given by $[\text{Pn}@\text{M}_{12}\text{Pn}_{10}]^{n-}$ and the remaining ligands Pn_5^- ($\text{Pn} = \text{As}, \text{Sb}$) was employed to study the bonding interactions between the central cluster and ligands. The numerical results are presented in Table 1. It is noteworthy that the EDA results on $[\text{Ti}(\eta^5\text{-P}_5)_2]^{2-}$ are in agreement with previous results²⁴. The bond strength between coordination centre $[\text{Pn}@\text{M}_{12}\text{Pn}_{10}]^{n-}$ and the ligand Pn_5^- is larger than that between Ti^0 and P_5^- in $[\text{Ti}(\eta^5\text{-P}_5)_2]^{2-}$ and close to that between Fe^{2+} and C_5H_5^- in $\text{Fe}(\eta^5\text{-C}_5\text{H}_5)_2$. For $[\text{As}@\text{Co}_{12}\text{As}_{10}(\text{As}_5)_2]^{4+}$, the orbital interactions contribute more to the metal–ligand bonding than the electrostatic interactions, whereas this trend is reversed for $[\text{Sb}@\text{Fe}_{12}\text{Sb}_{10}(\text{Sb}_5)_2]^{5-}$.

Conclusion

We report the synthesis and characterization of sandwich-type clusters $[\text{Pn}@\text{M}_{12}\text{Pn}_{10}(\text{Pn}_5)_2]^{4-/5-}$ ($\text{Pn} = \text{As}, \text{Sb}; \text{M} = \text{Co}, \text{Fe}$), where the icosahedral $[\text{Pn}@\text{M}_{12}]$ cores are ligand-flanked in analogy to classical mononuclear sandwich structures. These clusters are inorganic sandwich-type complexes containing a 3D interlayer, which bridge a conceptual gap between classical sandwich complexes and cluster-based homologues. We anticipate that these clusters may pave the way for the design and synthesis of other sandwich compounds involving a 3D coordination centre, providing the possibility of applying these inorganic sandwich-type complexes as building blocks, and making it possible to further explore their characteristics and ligand–core interplay at the nanometre scale.

Methods

All manipulations and reactions were performed under a nitrogen atmosphere using standard Schlenk or glovebox techniques. Ethylenediamine (Aldrich, 99%) and toluene (Aldrich, 99.8%) were freshly distilled from sodium/benzophenone. Acetonitrile (Aldrich, 99.8%) was distilled from CaH_2 under nitrogen and was stored under nitrogen prior to use. 18-crown-6, purchased from Sigma-Aldrich (98%), was dried in vacuum for 1 day prior to use. DPPF was purchased from Aladdin (97%) and was not further processed prior to use. The precursors K_5As_4 and K_5Sb_4 were synthesized by heating stoichiometric mixtures of the elements at 650 °C and 850 °C, respectively, for 30 h in sealed niobium containers jacketed in evacuated fused silica tubes according to previously reported synthetic procedures⁴¹. $\text{Co}(\text{PPh}_3)_2\text{Cp}$ was synthesized according to a reported method⁴².

Synthesis of $\{[\text{K}(\text{18-crown-6})]_2(\text{en})\}_2[\text{As}@\text{Co}_{12}\text{As}_{10}(\text{As}_5)_2]^{4+}$ (**1'**)

K_5As_4 (50 mg, 0.100 mmol) and 18-crown-6 (98 mg, 0.370 mmol) were dissolved in 2.5 ml en and stirred at 55 °C for 1 h to yield a greenish-brown solution. $\text{Co}(\text{PPh}_3)_2\text{Cp}$ (45 mg, 0.070 mmol) was added and stirred vigorously at 75 °C for 4 h. The resulting red-brown solution was centrifuged and filtered with standard glass wool, then carefully layered by 3 ml toluene. After 3 months, long black plate-like crystals of $\{[\text{K}(\text{18-crown-6})]_2(\text{en})\}_2[\text{As}@\text{Co}_{12}\text{As}_{10}(\text{As}_5)_2]^{4+}$ were observed in the test tube in approximately 14% yield overall.

Synthesis of $\{[\text{K}(\text{18-crown-6})]_2(\text{en})\}_2[\text{K}(\text{18-crown-6})]_2[\text{As}@\text{Co}_{12}\text{As}_{10}(\text{As}_5)_2]^{4+}$ (**2'**)

K_5As_4 (50 mg, 0.100 mmol) and 18-crown-6 (98 mg, 0.370 mmol) were dissolved in 2.5 ml en and stirred at 55 °C for 1 h to yield a greenish-brown solution. $\text{Co}(\text{PPh}_3)_2\text{Cp}$ (65 mg, 0.100 mmol) was added and stirred vigorously at 75 °C for 4 h. The resulting red-brown solution was centrifuged and filtered with standard glass wool, then carefully layered by 3 ml toluene. After 1 month, black block crystals of

Table 1 | EDA-NOCV results (in kcal mol⁻¹) of [As@Co₁₂As₁₀(As₅)₂]⁴⁻, [Sb@Fe₁₂Sb₁₀(Sb₅)₂]⁵⁻, Fe(η⁵-C₅H₅)₂ and [Ti(η⁵-P₅)₂]²⁻ at the PBE0-D3(BJ)/TZ2P level

Interacting fragments	[As@Co ₁₂ As ₁₀ (As ₅) ₂] ⁴⁻ (octet)	[Sb@Fe ₁₂ Sb ₁₀ (Sb ₅) ₂] ⁵⁻ (septet)	Fe(η ⁵ -C ₅ H ₅) ₂ (singlet)	[Ti(η ⁵ -P ₅) ₂] ²⁻ (singlet)
	Co ₁₂ As ₁₁ ²⁻ (octet) + (As ₅) ₂ ²⁻ (singlet)	Fe ₁₂ Sb ₁₁ ³⁻ (septet) + (Sb ₅) ₂ ²⁻ (singlet)	Fe ²⁺ (singlet) + (C ₅ H ₅) ₂ ²⁻ (singlet)	Ti ⁰ (singlet) + (P ₅) ₂ ²⁻ (singlet)
ΔE _{int}	-498.5	-858.5	-856.7	-359.8
ΔE _{Pauli}	+1947.6	+1873.3	+296.5	+340.1
ΔE _{disp}	-61.3	-67.9	-1.0	-4.7
ΔE _{elstat} ^a	-1267.1 (53.1%)	-1120.1 (42.0%)	-636.0 (55.2%)	-270.9 (39.0%)
ΔE _{orb} ^a	-1117.6 (46.9%)	-1543.7 (58.0%)	-516.2 (44.8%)	-424.3 (61.0%)

^aThe percentage values in parentheses give the contribution to the total attractive interactions ΔE_{elstat} (the electrostatic interaction) + ΔE_{orb} (the orbital interaction term).

{K₂[K(18-crown-6)](en)₂}[K(18-crown-6)]₂[As@Co₁₂As₁₀(As₅)₂] were observed in the test tube in approximately 12% yield.

Synthesis of [K₃(18-crown-6)₃(en)₂][K(18-crown-6)(en)]₂[Sb@Fe₁₂Sb₁₀(Sb₅)₂]_{0.745}[Sb@Fe₁₂@Sb₂₀]_{0.255} (3')

K₅Sb₄ (95 mg, 0.139 mmol) and 18-crown-6 (100 mg, 0.393 mmol) were dissolved in 2.5 ml en and stirred at 60 °C for 0.5 h to yield a brown solution. DPPF (38 mg, 0.069 mmol) was added and stirred vigorously at room temperature for 3 h. The resulting red-brown solution was centrifuged and filtered with standard glass wool, then carefully layered by 3 ml toluene. After 3 weeks, black block crystals of [K₃(18-crown-6)₃(en)₂][K(18-crown-6)(en)]₂[Sb@Fe₁₂Sb₁₀(Sb₅)₂]_{0.745}[Sb@Fe₁₂@Sb₂₀]_{0.255} were observed in the test tube in approximately 15% yield.

X-ray diffraction

Suitable single crystals of the title compounds were selected for X-ray diffraction analyses. Crystallographic data were collected on a Rigaku XtalAB Pro MM007 DW diffractometer with graphite-monochromated Cu Kα radiation (λ = 1.54184 Å). The structures of {[K(18-crown-6)]₂(en)}₂[As@Co₁₂As₁₀(As₅)₂] and {K₂[K(18-crown-6)](en)₂}[K(18-crown-6)]₂[As@Co₁₂As₁₀(As₅)₂] were solved using direct methods and then refined using SHELXL-2014 and Olex2 to convergence^{43–45}, in which all the non-hydrogen atoms were refined anisotropically during the final cycles. All hydrogen atoms of the organic molecule were placed by geometric considerations and were added to the structure factor calculation. Structure refinement details for [K₃(18-crown-6)₃(en)₂][K(18-crown-6)(en)]₂[Sb@Fe₁₂Sb₁₀(Sb₅)₂]_{0.745}[Sb@Fe₁₂@Sb₂₀]_{0.255} and all atoms were refined using anisotropic displacement parameters. The asymmetric unit contains two crystallographically independent half-clusters of [Sb@Fe₁₂Sb₁₀(Sb₅)₂]⁵⁻ (**3a**) and [Sb@Fe₁₂@Sb₂₀]⁵⁻ (**3b**). A summary of the crystallographic data for the title compounds is provided Supplementary Table 1 and selected bond distances are given in Supplementary Tables 2–4.

Theoretical methods

Geometry optimizations and subsequent calculations were performed with the ADF 2021 code⁴⁶ with the all-electron triple-ξ Slater basis set plus the double-polarization (STO-TZ2P) basis set in conjunction with the hybrid PBE0 functional^{47,48}. The bonding interactions were studied by using an EDA⁴⁹ together with the natural orbitals for chemical valence (NOCV)^{50,51}. The EDA-NOCV calculations were performed by using PBE0-D3(BJ) functional^{47,48,52} with the basis set TZ2P on PBE0/TZ2P-optimized geometries. The Hirshfeld charge analysis was also carried out in ADF 2021 code⁴⁶.

ESI-MS investigations

Negative-ion-mode ESI-MS of the acetonitrile solution of crystals of all samples was performed on an LTQ linear ion trap spectrometer (Agilent Technologies ESI-TOF-MS, 6230). The spray voltage was 5.48 kV and

the capillary temperature was kept at 300 °C. The capillary voltage was 30 V. The samples were prepared inside a glovebox and rapidly transferred to the spectrometer in an airtight syringe by direct infusion with a Harvard syringe pump at 0.2 ml min⁻¹.

EDX

EDX analysis was performed using a field emission scanning electron microscope (JEOL JSM-7800F). Data acquisition was performed with an acceleration voltage of 15 kV and an accumulation time of 60 s.

Data availability

Crystallographic data for the structures reported in this Article have been deposited at the Cambridge Crystallographic Data Centre, under deposition numbers CCDC 2204629 (**1'**), 2204630 (**2'**), 2204596 (**3'**). Copies of the data can be obtained free of charge via <https://www.ccdc.cam.ac.uk/structures/>. All other data supporting the findings of this study are available within the Article and its Supplementary Information.

References

- Kealy, T. J. & Pauson, P. L. A new type of organo-iron compound. *Nature* **168**, 1039–1040 (1951).
- Fischer, E. O. & Pfab, W. Cyclopentadien-Metallkomplexe, ein neuer Typ metallorganischer Verbindungen. *Z. Naturforsch. B 7*, 377–379 (1952).
- Wilkinson, G., Rosenblum, M., Whiting, M. C. & Woodward, R. B. The structure of iron bis-cyclopentadienyl. *J. Am. Chem. Soc.* **74**, 2125–2126 (1952).
- Togni, A. & Halterman, R. L. *Metallocenes: Synthesis Reactivity Applications* (Wiley, 1998).
- Gómez Arrayás, R., Adrio, J. & Carretero, J. C. Recent applications of chiral ferrocene ligands in asymmetric catalysis. *Angew. Chem. Int. Ed.* **45**, 7674–7715 (2006).
- Jaouen, G., Vessières, A. & Top, S. Ferrocifen type anti cancer drugs. *Chem. Soc. Rev.* **44**, 8802–8817 (2015).
- Luo, J., Hu, B., Hu, M., Wu, W. & Liu, T. L. An energy-dense, powerful, robust bipolar zinc-ferrocene redox-flow battery. *Angew. Chem. Int. Ed.* **61**, e202204030 (2022).
- Nakahata, M., Takashima, Y., Yamaguchi, H. & Harada, A. Redox-responsive self-healing materials formed from host-guest polymers. *Nat. Commun.* **2**, 511 (2011).
- Liu, J. et al. An organometallic super-gelator with multiple-stimulus responsive properties. *Adv. Mater.* **20**, 2508–2511 (2008).
- Mathey, F. Les phosphacymantrenes, premiers heterocycles phosphores d'une véritable chimie 'aromatique'. *Tetrahedron Lett.* **17**, 4155–4158 (1976).
- Maigrot, N., Avarvari, N., Charrier, C. & Mathey, F. Synthesis of 1,2-diphospholide ions. *Angew. Chem. Int. Ed.* **34**, 590–592 (1995).

- Bartsch, R., Hitchcock, P. B. & Nixon, J. F. First structural characterisation of penta- and hexa-phosphorus analogues of ferrocene. Synthesis, crystal and molecular structure of the air-stable, sublimable iron sandwich compounds $[\text{Fe}(\eta^5\text{-C}_2\text{R}_2\text{P}_3)_2]$, and $[\text{Fe}(\eta^5\text{-C}_3\text{R}_3\text{P}_2)(\eta^5\text{-C}_2\text{R}_2\text{P}_3)]$ (R=Bu^t). *J. Chem. Soc., Chem. Commun.* 1146–1148 (1987).
- Scherer, O. J., Hilt, T. & Wolmershäuser, G. $[\{\text{Cp}^{\text{R}}(\text{OC})_2\text{Fe}\}_2(\mu\text{-}\eta^1\text{-}\eta^1\text{-P}_4)]$: starting material for the synthesis of iron sandwich compounds with a 1,2,3-triphospholyl ligand and of a trinuclear iron complex with a P₁₁ ligand. *Angew. Chem. Int. Ed.* **39**, 1425–1427 (2000).
- Scherer, O. J. & Brück, T. $[(\eta^5\text{-P}_5)\text{Fe}(\eta^5\text{-C}_5\text{Me}_5)]$, a pentaphosphaferrocene derivative. *Angew. Chem. Int. Ed.* **26**, 59 (1987).
- Scheer, M., Deng, S., Scherer, O. J. & Sierka, M. Tetrakisphosphacyclopentadienyl and triphosphaallyl ligands in iron complexes. *Angew. Chem. Int. Ed.* **44**, 3755–3758 (2005).
- Heinl, C. et al. The missing parent compound $[(\text{C}_5\text{H}_5)\text{Fe}(\eta^5\text{-P}_5)]$: synthesis, characterization, coordination behavior and encapsulation. *Chemistry* **27**, 7542–7548 (2021).
- Peresyphkina, E., Virovets, A. & Scheer, M. Organometallic polyphosphorus complexes as diversified building blocks in coordination chemistry. *Coord. Chem. Rev.* **446**, 213995 (2021).
- Giusti, L. et al. Coordination chemistry of elemental phosphorus. *Coord. Chem. Rev.* **441**, 213927 (2021).
- Urne, E., Brennessel, W. W., Cramer, C. J., Ellis, J. E. & von Ragué Schleyer, P. A carbon-free sandwich complex $[(\text{P}_5)_2\text{Ti}]^{2-}$. *Science* **295**, 832–834 (2002).
- Wang, Z. C., Qiao, L., Sun, Z. M. & Scheer, M. Inorganic ferrocene analogue $[\text{Fe}(\text{P}_4)_2]^{2-}$. *J. Am. Chem. Soc.* **144**, 6698–6702 (2022).
- Scherer, O., Blath, C. & Wolmershäuser, G. Ferrocene mit einem Pentaarsacyclopentadienyl-Liganden. *J. Organomet. Chem.* **387**, C21–C24 (1990).
- Breunig, H. J., Burford, N. & Rösler, R. Stabilization of a pentastibacyclopentadienyl ligand in the triple-decker sandwich complexes $[\{(\eta^5\text{-1,2,4-}^t\text{Bu}_3\text{C}_5\text{H}_2)\text{Mo}\}_2(\mu, \eta^5\text{-Sb}_3)]$ and $[(\eta^5\text{-1,2,4-}^t\text{Bu}_3\text{C}_5\text{H}_2)\text{Mo}(\mu, \eta^5\text{-Sb}_3)\text{Mo}(\eta^5\text{-1,4-}^t\text{Bu}_2\text{-2-MeC}_5\text{H}_2)]$. *Angew. Chem. Int. Ed.* **39**, 4148–4150 (2000).
- Scherer, O. J., Wiedemann, W. & Wolmershäuser, G. $[(\eta^5\text{-C}_5\text{H}_4\text{R})(\text{CO})_3\text{Cr}]_2\text{Cr}(\mu, \eta^5\text{-As}_5)\text{Cr}(\eta^5\text{-C}_5\text{H}_4\text{Me})]$, ein Tripeldecker-Sandwichkomplex mit unverzerrtem cyclo-As₅-Mitteldeck. *J. Organomet. Chem.* **361**, C11–C14 (1989).
- Lein, M., Frunzke, J. & Frenking, G. Structures and bonding of the sandwich complexes $\text{Ti}(\eta^5\text{-E}_5)_2$ (E=CH, N, P, As, Sb): a theoretical study. *Inorg. Chem.* **42**, 2504–2511 (2003).
- Frunzke, J., Lein, M. & Frenking, G. Structures, metal–ligand bond strength, and bonding analysis of ferrocene derivatives with group-15 heteroligands $\text{Fe}(\eta^5\text{-E}_5)_2$ and $\text{FeCp}(\eta^5\text{-E}_5)$ (E=N, P, As, Sb). A theoretical study. *Organometallics* **21**, 3351–3359 (2002).
- Murahashi, T. et al. Discrete sandwich compounds of monolayer palladium sheets. *Science* **313**, 1104–1107 (2006).
- Teramoto, M. et al. Three-dimensional sandwich nanocubes composed of 13-atom palladium core and hexakis-carbocycle shell. *J. Am. Chem. Soc.* **140**, 12682–12686 (2018).
- Pan, F. X. et al. An all-metal aromatic sandwich complex $[\text{Sb}_3\text{Au}_3\text{Sb}_3]^{3-}$. *J. Am. Chem. Soc.* **137**, 10954–10957 (2015).
- Xu, H. L. et al. A sandwich-type cluster containing $\text{Ge}@Pd_3$ planar fragment flanked by aromatic nonagermanide caps. *Nat. Commun.* **11**, 5286 (2020).
- Spiekermann, A., Hoffmann, S. D., Kraus, F. & Fässler, T. F. $[\text{Au}_3\text{Ge}_{18}]^{5-}$ —a gold–germanium cluster with remarkable Au–Au interactions. *Angew. Chem. Int. Ed.* **46**, 1638–1640 (2007).
- Moses, M. J., Fettinger, J. C. & Eichhorn, B. W. Interpenetrating As_{20} fullerene and Ni_{12} icosahedra in the onion-skin $[\text{As}@Ni_{12}@As_{20}]^{3-}$ ion. *Science* **300**, 778–780 (2003).
- Wang, Y. et al. $\text{Sb}@Ni_{12}@Sb_{20}^{-/n}$ and $\text{Sb}@Pd_{12}@Sb_{20}^{-/n}$ cluster anions, where $n = +1, -1, -3, -4$: multi-oxidation-state clusters of interpenetrating platonic solids. *J. Am. Chem. Soc.* **139**, 619–622 (2017).
- Li, Z. Y. et al. Counterion-induced crystallization of intermetallic matryoshka clusters $[\text{Sb}@Pd_{12}@Sb_{20}]^{3-/4-}$. *Dalton Trans.* **46**, 3453–3456 (2017).
- Stegmaier, S. & Fässler, T. F. A bronze matryoshka: the discrete intermetallic cluster $[\text{Sn}@Cu_{12}@Sn_{20}]^{12-}$ in the ternary phases $\text{A}_{12}\text{Cu}_{12}\text{Sn}_{20}$ (A=Na, K). *J. Am. Chem. Soc.* **133**, 19758–19768 (2011).
- Jinlong, Y., Chuanyun, X., Shangda, X. & Kelin, W. Stability, electronic and magnetic properties, and reactivity of icosahedral MCo_{12} clusters. *Phys. Rev. B* **48**, 12155–12163 (1993).
- Zhang, H., Cui, C. & Luo, Z. The doping effect of 13-atom iron clusters on water adsorption and O–H bond dissociation. *J. Phys. Chem. A* **123**, 4891–4899 (2019).
- Moses, M. J., Fettinger, J. C. & Eichhorn, B. W. $[\text{Ni}_5\text{Sb}_{17}]^{4+}$ transition-metal Zintl ion complex: crossing the Zintl border in molecular intermetallic clusters. *Inorg. Chem.* **46**, 1036–1038 (2007).
- Ruiz-Martínez, A., Casanova, D. & Alvarez, S. Polyhedral structures with an odd number of vertices: nine-coordinate metal compounds. *Chemistry* **14**, 1291–1303 (2008).
- Walter, M. et al. A unified view of ligand-protected gold clusters as superatom complexes. *Proc. Natl Acad. Sci. USA* **105**, 9157–9162 (2008).
- Wei, J. et al. Looking at platinum carbonyl nanoclusters as superatoms. *Nanoscale* **14**, 3946–3957 (2022).
- Gascoin, F. & Sevov, S. C. Synthesis and characterization of the ‘metallic salts’ A_5Pn_4 (A=K, Rb, Cs and Pn=As, Sb, Bi) with isolated zigzag tetramers of Pn_4^{4-} and an extra delocalized electron. *Inorg. Chem.* **40**, 5177–5181 (2001).
- Wakatsuki, Y., Yamazaki, H., Lindner, E. & Bosamle, A. 1,3-Butadiene-1,4-diyl(η^5 -cyclopentadienyl)-(triphenylphosphine) cobalt with various substituents. *Inorg. Synth.* **26**, 189–200 (1989).
- Sheldrick, G. M. SHELXT—integrated space-group and crystal-structure determination. *Acta Crystallogr. A* **71**, 3–8 (2015).
- Dolomanov, O. V., Bourhis, L. J., Gildea, R. J., Howard, J. A. K. & Puschmann, H. OLEX2: a complete structure solution, refinement and analysis program. *J. Appl. Crystallogr.* **42**, 339–341 (2009).
- Spek, A. L. Structure validation in chemical crystallography. *Acta Crystallogr. D* **65**, 148–155 (2009).
- te Velde, G. et al. Chemistry with ADF. *J. Comp. Chem.* **22**, 931–967 (2001).
- Ernzerhof, M. & Scuseria, G. Assessment of the Perdew–Burke–Ernzerhof exchange–correlation functional. *J. Chem. Phys.* **110**, 5029 (1999).
- Adamo, C. & Barone, V. Physically motivated density functionals with improved performances: the modified Perdew–Burke–Ernzerhof model. *J. Chem. Phys.* **116**, 5933 (2002).
- Ziegler, T. & Rauk, A. On the calculation of bonding energies by the Hartree Fock Slater method. *Theor. Chim. Acta* **46**, 1–10 (1977).
- Mitoraj, M. & Michalak, A. Applications of natural orbitals for chemical valence in a description of bonding in conjugated molecules. *J. Mol. Model.* **14**, 681–687 (2008).
- Mitoraj, M. P., Michalak, A. & Ziegler, T. A combined charge and energy decomposition scheme for bond analysis. *J. Chem. Theory Comput.* **5**, 962–975 (2009).
- Grimme, S., Ehrlich, S. & Goerigk, L. Effect of the damping function in dispersion corrected density functional theory. *J. Comput. Chem.* **32**, 1456–1465 (2011).

Acknowledgements

This work was supported by the National Natural Science Foundation of China (92161102, 21971118 and 22003048) and the Natural Science Foundation of Tianjin City (numbers 21JCZXJC00140 and 20JCYBJC01560) to Z.-M.S. Z.-M.S. thanks the 111 project (B18030) from China (MOE). A.M.C. thanks ANID for regular grant 1221676.

Author contributions

Z.-M.S. conceived and directed the research. X.-H.Y. synthesized compounds **1'** and **2'**. W.-X.C. synthesized compound **3'**. A.M.-C. and T.Y. performed the computational studies. X.-H.Y. and W.-X.C. performed the single-crystal X-ray diffraction, EDX and ESI-MS, and analysed the data. All authors co-wrote the manuscript.

Competing interests

The authors declare no competing interests.

Additional information

Supplementary information The online version contains supplementary material available at <https://doi.org/10.1038/s44160-023-00247-0>.

Correspondence and requests for materials should be addressed to Zhong-Ming Sun.

Peer review information *Nature Synthesis* thanks Giovanni Maestri and the other, anonymous, reviewer(s) for their contribution to the peer review of this work. Primary handling editor: Alison Stoddart, in collaboration with the *Nature Synthesis* team.

Reprints and permissions information is available at www.nature.com/reprints.

Publisher's note Springer Nature remains neutral with regard to jurisdictional claims in published maps and institutional affiliations.

Springer Nature or its licensor (e.g. a society or other partner) holds exclusive rights to this article under a publishing agreement with the author(s) or other rightsholder(s); author self-archiving of the accepted manuscript version of this article is solely governed by the terms of such publishing agreement and applicable law.

© The Author(s), under exclusive licence to Springer Nature Limited 2023